Appendix A. STEREO/SECCHI/HI Calibration and Measurement Algorithms Document (CMAD)

Version 1.0 / 30 June 2021 – Initial release

Version 1.1 / 06 December 2021 – Updated references

A.1 Introduction

Alongside EUVI, COR1 and COR2, the Heliospheric Imager (HI) instruments form an integral component of the Sun Earth Connection Coronal and Heliospheric Investigation (SECCHI) instrument suite aboard the twin Solar Terrestrial Relations Observatory (STEREO) spacecraft. The near-identical HI instruments, mounted on the side facing the Sun-Earth line on each STEREO spacecraft, comprise two broad-band visible-light refracting camera systems (HI-1 and HI-2) – based on radiatively-cooled charge-coupled device (CCD)-based detectors – housed in an array of forward, perimeter and internal baffles. This complex baffle system is designed to minimize stray light to a level whereby the faint Thomson-scattered signal from the solar wind plasma, and the coronal mass ejections therein, can be detected. Figure 1 presents the design concept of the HI instrument, taken from Eyles et al. (2009), showing the camera placement deep in the baffle system, as well as other salient instrument components. The one-shot HI door, utilized to protect the optical and baffle systems during ground operations, launch, and the initial cruise phase activities, was opened on 13 December 2006, on STEREO-A, and 11 January 2007, on STEREO-B.

Each inner (HI-1) camera has a 20° x 20° field-of-view, the boresight of which is, in nominal operations, aligned at 14° elongation (angle from Sun-center) in the ecliptic plane. The boresight of the 70° field-of-view outer (HI-2) cameras is aligned, again in nominal operations, at 53.7° elongation. Thus, between them, the HI cameras on each STEREO spacecraft provide elongation coverage extending from 4° to 88.7° along the Sun-Earth line; the inner edge of this combined HI field-of-view is closely matched to the outer field of view of the COR2 instrument. A summary of the HI instruments is given by Howard *et al*. (2008); for a more complete description, the reader is directed to Eyles et al. (2009).

The goal of HI is to study the evolution of coronal mass ejections (CMEs) as they propagate through the inner heliosphere, out to Earth-like distances and beyond. These measurements, combined with those from EUVI, COR1 and COR2, aim to answer the questions:

- What is the timing of physical properties involved in CME initiation? What are the structures involved in CME initiation?
- What is the 3-dimensional structure and kinematic properties of CMEs?
- What is the 3-dimensional structure of active regions, coronal loops, helmet streamers, etc.?
- What are the critical forces controlling the properties of CMEs in the corona and interplanetary medium?

The spectral passband of the HI-1 cameras is 630 to 730 nm, to match that of COR2; an even wider passband, 400 to 1000 nm, is used for HI-2 in order to achieve the signal-to-noise ratio necessary to discern the faint solar wind signal. Notwithstanding their broad-band design, a long integration time is also required for the HI cameras, noting that a CME is typically only 1% of the brightness of the major

background sources – namely the F-corona and the brighter stars – in the HI field-of-view. To this end, each HI image comprises the sum of multiple shorter exposures, 30 40-second exposures in the case of HI-1 imagery and 99 50-second exposures in the case of HI-2. The nominal cadence is 40 minutes and 120 minutes for HI-1 and HI-2 science images, respectively. Each exposure is scrubbed of energetic particles signatures – cosmic rays and solar energetic particles – prior to summing, as the accumulated effect of energetic particle contamination over such a long integration time would be significant, even during quiet conditions.

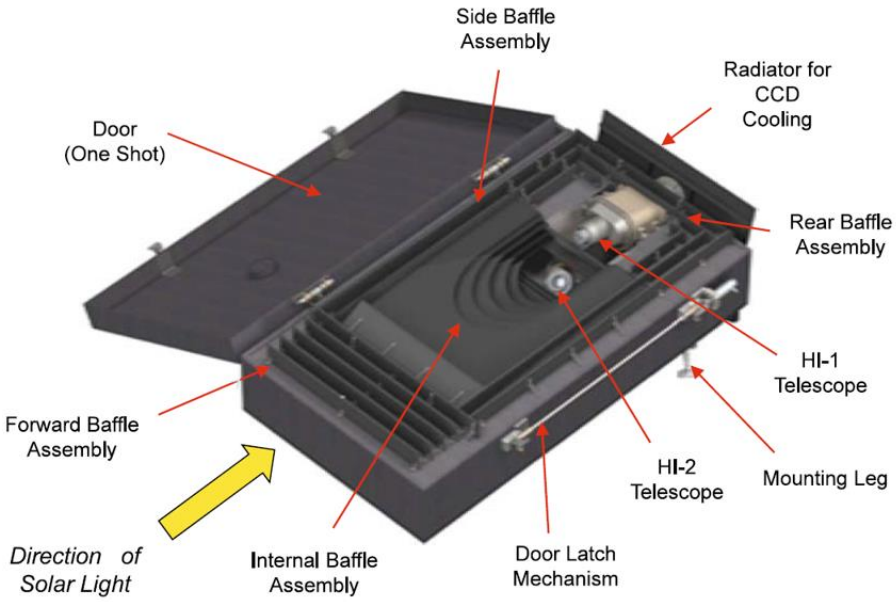

Figure 1. HI instrument design concept.

A 2k x 2k pixel CCD, with 15µ detectors, yields a pixel size of 35 arcsec and 2 arcmin for the 20° and 70° field-of-view of the inner, HI-1, and outer, HI-2, cameras, respectively. After energetic particle scrubbing, exposures are binned 2 x 2, resulting in an image bin size of 70 arcsec for HI-1 and 4 arcmin for HI-2. The wide-angle nature of the HI-2 cameras, in particular, results in significant geometrical distortion from the standard gnomic projection assumed for most solar instruments. This distortion, while characterized pre-launch on ground, has been refined in-flight through comparison with a star map. Indeed, inclusion of the camera distortion ascertained in this way is part of the standard HI pipeline processing undertaken to ascertain the accurate pointing for each HI image taken in flight. Similarly, comparison with the magnitudes of selected, non-variable, stars has been used to refine the on-ground HI photometric calibration parameters; such analysis has demonstrated that the degradation of the HI cameras over the first 7 years of the mission was less than 0.1% per year. This trend is likely to have continued, however due to the degraded stability that accompanied the switching-off of the attitude control gyros, on 18 September 2013 and 7 January 2014 for STEREO-A and STEREO-B, respectively, such accurate photometric calibration is no longer easily achievable.

As noted above, the solar wind is of order 1% of the background signal at the elongations of HI, necessitating careful background determination to reveal the faint signatures of CMEs and other solar wind phenomena. Standard processing of HI data to Level 2 yields two background-subtracted products, the first, with a short timescale background removed (1-day background for HI-1 and 3-days for HI-2)

and the second, with an 11-day background subtracted in order to study the morphology and evolution of more stable features such as the background corona.

The aforementioned calibrations, and corrections, applied to HI imagery are described in the following sections of this Appendix, as listed below.

Section A.2	Photometric calibration
Section A.3	Geometric calibration
Section A.4	Background determination

A.1.1 Purpose

This document describes the photometric and geometric corrections used to convert from raw HI Level 0 images to calibrated Level 1 images, and the subsequent determination of the background for background-subtracted Level 2 products. The Level 0 data are stored in FITS format, as described in [**PIPELINE**]. All calibration files are distributed as part of the SECCHI software package in SolarSoft.

A.1.2 Contents

Section A.2 describes the procedure used to convert the HI data from raw Level 0 units (data numbers, DN) to a variety of calibrated Level 1 units – specifically DNS (DNs/pixel/sec), mean solar brightness (MSB), and S10 units – which is the basic step that underpins subsequent scientific analysis. Section A.3 describes the geometric calibration of the data, and its implementation. Section A.4 describes the procedure used for estimating the F-coronal and instrumental background.

A.1.3 References

[PIPELINE] STEREO/SECCHI Level-0 to Level-0.5 FITS Pipeline CMAD, STEREO_SECCHI_Reduce_CMAD_20211206.pdf, Version 1.1, 06 December 2021

Eyles, C. J., Harrison, R. A., Davis, C. J., Waltham, N. R., Shaugnessy, B. M., Mapson-Menard, H. C. A., Bewsher, D., Crothers, S. R., Davies, J. A., Simnett, G. M., Howard, R. A., Moses, J. D., Newmark, J. S., Socker, D. G., Halain, J. -P., Defise, J. -M., Mazy, E., Rochus, P., 2009, The Heliospheric Imagers onboard the STEREO mission, *Solar Phys.*, **254**, 387–445.

Howard, R. A., Moses, J. D., Vourlidas, A., Newmark, J. S., Socker, D. G., Plunkett, S. P.; Korendyke, C. M., Cook, J. W., Hurley, A., Davila, J. M., Thompson, W. T., St Cyr, O. C.; Mentzell, E., Mehalick, K., Lemen, J. R., Wuelser, J. P., Duncan, D. W., Tarbell, T. D.; Wolfson, C. J., Moore, A. Harrison, R. A., Waltham, N. R., Lang, J., Davis, C. J.; Eyles, C. J., Mapson-Menard, H., Simnett, G. M., Halain, J. P., Defise, J. M., Mazy, E.; Rochus, P., Mercier, R., Ravet, M. F., Delmotte, F., Auchere, F., Delaboudiniere, J. P.; Bothmer, V., Deutsch, W., Wang, D., Rich, N., Cooper, S., Stephens, V., Maahs, G.; Baugh, R., McMullin, D., Carter, T., 2008, Sun Earth Connection Coronal and Heliospheric Investigation (SECCHI), *Space Sci. Rev.*, **136**, 67–115.

A.2 Photometric calibration

A.2.1 Overview

The initial photometric calibration of the HI instruments was performed via modelling and from laboratory measurements taken prior to launch (Eyles at al. 2009). This has since been refined using measurements of stars during operation. For HI-1 this was first done by Bewsher *et al.* (2010) and Bewsher, Brown & Eyles (2012). A similar analysis for HI-2 was carried out by Tappin, Eyles & Davies (2015). The time evolution of the calibration parameters was determined by Tappin, Eyles & Davies (2017).

A.2.1.1 Heritage

The HI photometric calibration, both on-ground and in-flight, is based on procedures developed over many years for similar visible-light instruments, on the Helios, SOHO and Coriolis missions.

A.2.1.2 Product Description

HI images are generated by taking a series of short exposures and then binning and summing them to produce the 1024 × 1024 images that are downlinked. This necessitates a certain level of on-board processing, which is described in detail by Eyles *et al.* (2009; section 5.3). In summary:

1. The electronic bias is determined from the CCD underscan columns and subtracted.
2. Energetic particle hits are removed (scrubbed) by comparison with the previous exposure.
3. The underscan and overscan regions are trimmed
4. The exposures are binned 2 × 2 from the original 2048 pixel square exposures to 1024 image bins square.
5. The exposures are summed. For HI-1, 30 exposures are summed to produce an image every 40 minutes. For HI-2, 99 exposures are summed to produce one image every two hours. The number of particle hits detected for each exposure are stored in the final, row of the image.

The resulting 24-bit images are downlinked as the Level 0 data.

After the downlinked telemetry stream has been reassembled to form the Level 0 images, a number of further operations are performed to produce the Level 1 images that are useful for analysis. This processing is described by Eyles et al. (2009; section 10). The determination of the unit conversion parameters and flat field are described by Bewsher et al. (2010), Bewsher, Brown & Eyles (2012) and Tappin, Eyles & Davies (2017) for HI-1 and by Tappin, Eyles & Davies (2015, 2017) for HI-2. In summary:

1. Remove the energetic particle scrubbing values from the final row of the image, replacing the values in these bins with values from the adjacent row.
2. Identify saturated columns and missing data blocks, and insert appropriate data values (NaNs for saturation, interpolated values for missing blocks).
3. Apply the correction for shutterless readout of the cameras (see Section A.2.1.1).
4. Apply a flat-field correction to the image (see Section A.3.2.3).
5. Correct the pointing and optics parameter values in the headers.
6. Since superior conjunction, the images are rotated to place north at the top.

The calibrated images for HI are supplied in three sets of units:

- DN per CCD pixel per second (DNS).
- MSB (the mean surface brightness of the solar disk).
- S10 units (the brightness of m_v = 10 star of solar type per square degree).

The MSB and S10 images are corrected for the variation in pixel solid angle across the field of view (see Appendix A.3 for more information). Thus the count-rate (DNS) images are more suitable for astronomical studies focused on point sources, while the MSB and S10 images are appropriate for studies of the solar wind, zodiacal light etc.

The background subtraction methods used to generate the Level 2 data are described below in Appendix A.4.

A.2.2 Theoretical Description

The basic process of converting from raw DNS to calibrated MSB can be described as follows

$$C_{MBS} = \frac{n_{pix}}{I_{sun}}$$

where C_{MBS} is the conversion factor (MSB/pixel), n_{pix} is the solid angle of the Sun expressed in pixels and

$$I_{sun} = \frac{A}{G}\frac{1}{hc}\int_0^\infty \lambda\, F_{sun}(\lambda) T(\lambda) d\lambda$$

is the intensity of the Sun in DN/s [A is the area of the aperture, G is the electronic gain (= 15 photo-electrons per DN), $F_{sun}(\lambda)$ is the spectral intensity of the Sun and $T(\lambda)$ is the net efficiency of the instrument (optical transmission multiplied by detector QE)].

The conversion factor to S10/pixel is similar where n_{pix} is now the number of pixels within one square degree and I_{sun} is replaced by $I_{10} = I_{sun} \times 10^{-36.74/2.5}$.

A.2.2.1 Shutterless Correction

Before each scheduled exposure, the CCD is cleared row by row. As the CCD is exposed to the sky scene during this clear, each row accumulates charge based on the clear step time (CLEARTIM in the SECCHI header). The imaging area of the CCD is then held stable for the exposure time (EXPTIME) and is then read out row by row. Similarly, during readout, the CCD is also still accumulating charge, this time based on the read step time (READTIME). For further details see Eyles et al. (2009; section 10.1.2).

The net effect of this is that the recorded exposure is a product of the observation and a matrix where every cell on the diagonal is EXPTIME, on one side of this every cell contains CLEARTIM and on the other side, READTIME, i.e. we define a time weighting matrix $\boldsymbol{T}$ such that

$$\|T\| = \begin{pmatrix} T_{exp} & T_{clear} & \cdots & \cdots & \cdots & T_{clear} \\ T_{read} & T_{exp} & T_{clear} & \cdots & \cdots & T_{clear} \\ \vdots & \vdots & \vdots & \vdots & \vdots & \vdots \\ T_{read} & T_{read} & \cdots & \cdots & T_{exp} & T_{clear} \\ T_{read} & T_{read} & \cdots & \cdots & \cdots & T_{exp} \end{pmatrix},$$

then

$$\left\|I^{(corrected)}\right\| = \|T^{-1}\| \times \left\|I^{(raw)}\right\|.$$

Multiplying the recorded exposure by the inverse of this matrix would, assuming a true square wave response on the CCD, return the observation in terms of counts that would have been received in a single second.

This is made slightly more complicated as the science data are binned 2 x 2 on-board, whereas the shutterless correction is carried out on the ground. So the cells along the main diagonal of ***T*** now actually include a combination of EXPTIME, CLEARTIM and READTIM. That said, the basic pattern is the same with common values on the main diagonal and two different values below and above this.

Because the weighting matric ***T*** is highly symmetric, it's possible to supply an analytic solution to the matrix inversion problem which greatly simplifies the shutterless correction process. This analytic solution is implemented by the routine sc_inverse.pro found under $SSW/stereo/secchi/idl/prep/hi. The basic method is as follows:

For a weighting matrix ***T*** of size ***N***x***N***, let ***DIAG*** represent the values along the diagonal, ***ABOVE*** represent the values above the diagonal, and ***BELOW*** represent the values below the diagonal. The inverse matrix ***P*** can then be calculated via the following algorithm (in IDL notation).

```
wt_above=double(above)/diag
wt_below=double(below)/diag

wt_above_1=wt_above-1
wt_below_1=wt_below-1

power_above=dblarr(n-1)
power_below=dblarr(n-1)

power_above[0]=1
power_below[0]=1

for row=1,n-2 do begin
   power_above[row]=power_above[row-1]*wt_above_1
   power_below[row]=power_below[row-1]*wt_below_1
end

v= [ 0 , wt_below *(power_below*reverse(power_above))]
u= [ 0 , wt_above *(power_above*reverse(power_below))]
```

```
d = -u[1]/wt_above - (total(v)-v[N-1])
f = 1/(diag*(d+wt_above*total(v)))

u[0]=d
v[0]=d
u=u*f
v=reverse(v)*f
p=dblarr(n,n,/nozero)
p[0,0]=u
for row=1,n-2 do begin
        p[0,row]=v[n-row-1:n-2]
        p[row,row]=u[0:n-row-1]
end
p[0,n-1]=v
```

This procedure is much faster than a standard matrix inversion routine.

A.2.3 Calibration and Validation

A.2.3.1 Calibration

The initial calibration was a combination of modelling and laboratory measurements carried out at Centre Spatial de Liège (CSL, Eyles et al. 2009).

In flight calibration, including the determination of the evolution of the instrument performance has been carried out using measurements of stars (Bewsher et al*.,* 2010; Bewsher, Brown & Eyles, 2012; Tappin Eyles & Davies, 2015, 2017).

A.2.3.2 Validation

The photometric calibration is validated by close correspondence with pre-launch modeled values and against stars with known stellar brightness.

A.2.4 References

Bewsher, D., Brown, D.S., Eyles, C.J.: 2012, Long-term evolution of the photometric calibration of the STEREO Heliospheric Imagers: I. HI-1, *Solar Phys*. **276**, 491-499.

Bewsher, D., Brown, D.S., Eyles, C.J., Kellet, B.J., White, G.J., Swinyard, B.: 2010, Determination of the photometric calibration and large-scale flatfield of the STEREO Heliospheric Imagers: I. HI-1, *Solar Phys.* **264**, 433-460.

Eyles, C.J., Harrison, R.A., Davis, C.J., Waltham, N.R., Shaughnessy, B.M., Mapson-Menard, H.C.A., Bewsher, D., Crothers, S.R., Davies, J.A., Simnett, G.M., Howard, R.A., Moses, J.D., Newmark, J.S., Socker, D.G., Halain, J.-P., Defise, J.-M., Mazy, E., Rochus, P.: 2009, The Heliospheric Imagers onboard the STEREO mission, *Solar Phys*. **254**, 387-445.

Tappin, S. J., Eyles, C. J., Davies, J. A., 2015, Determination of the photometric calibration and large-scale flatfield of the STEREO Heliospheric Imagers: II. HI-2, *Solar Phys*, **290**, 2143-2170.

Tappin, S. J., Eyles, C. J., Davies, J. A., 2017, On the long-term evolution of the sensitivity of the STEREO HI-1 cameras, *Solar Phys*, **292**, 28.

A.3 Geometric calibration

A.3.1 Overview

The initial geometric calibration of the HI instruments was done by modelling and from calibrations prior to launch (Eyles *at al.,* 2009, Halain 2012). This has since been refined using measurements of background stars during science mission operations.

For HI-1 this has been done by Brown, Bewsher & Eyles (2009) and Bewsher *et al.* (2010). A similar analysis for HI-2 has been carried out by Tappin, Eyles & Davies (2015).

A.3.1.1 Heritage

Since the HI instruments are the first of their kind there is no heritage of the analysis of data from similar instruments for wide-angle heliospheric imaging which we can draw upon.

A.3.1.2 Product Description

A method is employed that derives the instrument pointing solutions, along with other optical parameters, by comparing the locations of stars identified in HI images with known star positions. For the vast majority of images, a good attitude solution has been obtained with a mean-squared deviation between the observed and predicted star positions of one image pixel or less. Updated values have been obtained for the instrument offsets relative to the spacecraft, and for the optical parameters of the HI cameras. With this method the HI images can be considered as "self-calibrating," with the actual instrument offsets calculated as a byproduct. The updated pointing results and their by-products have been implemented in SolarSoft.

A.3.2 Theoretical Description

There are 3 aspects to the geometric calibration of the HI instruments:

- Calibration of the pointing offsets of the cameras relative to spacecraft attitude parameters.
- Correction for image distortion.
- Large-scale flat-field correction.

A.3.2.1 Camera Pointing Offsets

The methodology used here (see Brown, Bewsher & Eyles, 2009) is as follows:

1. Use spacecraft attitude parameters together with HI nominal pointing offsets to derive initial HI pointing estimates H_{yaw}, H_{pitch}, $H_{roll.}$
2. Identify stars from a star catalogue in the HI image (also using initial distortion parameter μ and paraxial focal length F_p, see below).

3. Calculate mean-square radial deviation between predicted and observed stars.
4. Perturb values of H_{yaw}, H_{pitch}, H_{roll}, μ and F_p until minimum mean-square deviation is found.
5. Use these optimized values for updating the pointing and image parameters in the headers of Level 1 images.

A.3.2.2 Correction for Image Distortion

Traditionally, almost all solar imaging instruments, including coronagraphs, have used the *gnomonic* or *tan* projection. In this projection, an object at an angle α to the instrument optical axis is projected onto the image plane at a radial distance r from image center given by:

$$r = F \tan \alpha$$

where F is the focal length.

However, this representation is not adequate to describe the imaging properties of the HI cameras because of their wide-angle optics and the resultant distortion at the edge of the field-of-view, particularly in the case of HI-2.

Analysis of results from scans of the calibration source across the fields-of-view obtained during pre-launch calibrations showed that the image projection of both cameras can be accurately represented by the relationship:

$$r = F_p (\mu + 1) \sin \alpha) / (\mu + \cos \alpha)$$

where F_p is the paraxial focal length and μ is a distortion parameter (Note that this reverts to the *tan* projection in the case $\mu = 0$)

The above relationship characterizes the Azimuthal Perspective (AZP) projection as derived by Calabretta & Greise, 2002. However, there is no particular physical basis for applying this projection to the HI cameras, the relationship is used simply because it is a suitable model which can accurately represent the behavior of the optics, including the distortion at the edges of the field-of-view.

The photometric conversion applied to Level 2 data for diffuse sources needs to take into account the variation in the solid angle subtended by a pixel across the FOV resulting from the AZP projection (see Bewsher, Brown & Eyles, 2010). Differentiating the above equation with respect to α we find:

$$F_p (d\alpha/dr) = (\mu + \cos \alpha)^2 / [(\mu + 1) (\mu \cos \alpha + 1)]$$

which leads to a correction to the conversion factor from DNS to MSB given by:

$$C_{MSB} (\alpha) = C_{MSB} ((\mu + 1) (\mu \cos \alpha + 1))^2 / (\mu + \cos \alpha)^4$$

where C_{MSB} is the on-axis photometric conversion factor.

A similar correction applies to the conversion from DNS to S10 units.

A.3.2.3 Large-Scale Flat-Field Correction

Preliminary large-scale flat-field corrections for the HI-B cameras obtained during pre-launch calibrations at CSL were fitted to polynomials of type:

$$I = I_0 (1 + a\, r^2 + b\, r^4)$$

where I is the response as a function of distance r from the center of the CCD image and I_0 is the response on axis (CCD center).

The correction to be applied is then simply:

$$I_{corr} = I_{meas} / (1 + a\, r^2 + b\, r^4)$$

where I_{meas} is the measured signal in an image bin and I_{corr} is its corrected value.

In the case of HI-1, this approach was subsequently replaced by look-up tables of correction factors for every image bin, derived from in-orbit observations of stars (see Bewsher et al., 2010).

In the case of HI-2, the above 2-parameter polynomial correction was subsequently replaced by a 5-parameter correction of the form:

$$I / I_0 = a_0 + a_1\, r^2 + a_2\, r^4 + a_3 \max (r - a_4, 0)^2$$

(see Tappin, Eyles & Davies, 2015).

A.3.3 Calibration and Validation

A.3.3.1 Calibration

Pre-launch calibration of the HI instruments was performed at CSL (see Eyles at al., 2009 and Halain 2012). The instrument was installed in a 3m diameter vacuum chamber, and was mounted on a remotely-controlled rotary platform so that it could be rotated about a vertical axis. This allowed a horizontal light beam from a collimator to be scanned across the center-line of the HI-1 and HI-2 fields-of-view, corresponding to the direction of the ecliptic (it was only possible to scan in one direction).

A summary of the principal optical calibration parameters obtained in the pre-launch calibrations appears below:

Parameter	HI-1A	HI-2A	HI-1B	HI-2B
Paraxial focal length, F_p (mm)	77.54	21.46	77.65	21.52
Paraxial plate scale (arcsec per pixel)	35.92	129.8	35.87	129.4
Distortion parameter, μ	0.167	0.833	0.100	0.651
Flat field parameter, a (mm^{-2})	*	*	-2.18×10^{-4}	-6.24×10^{-4}
Flat field parameter, b (mm^{-4})	*	*	$< 10^{-12}$	-1.65×10^{-6}

* No values obtained for HI-A due to schedule constraints, HI-B values assumed for initial calibrations

Figure 2, below, shows the fits to the AZP projection with the above values of μ obtained for the HI-B cameras. The vertical axis represents the distortion expressed as the angular deviation from a linear plate-scale. The available data points for HI-2B are limited by the presence of an Earth occulter in front of the CCD on the centerline of the field-of-view.

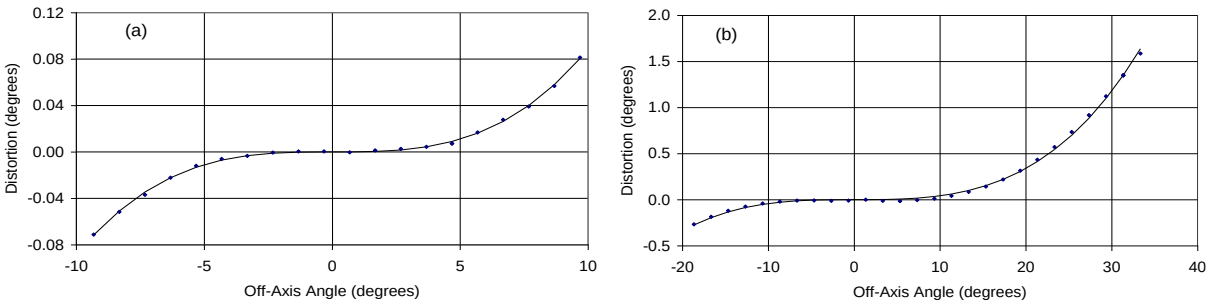

Figure 2. Fits to the AZP projection.

The following updates to the pre-launch calibrations have been made using in-orbit observations of stars, as follows:

- Brown, Bewsher & Eyles (2009) used fits to star positions in the NOMAD catalog (Zacharias *et al*., 2004) to update the pointing offsets relative to spacecraft attitude parameters and to provide updated values for the distortion parameter μ for all 4 cameras.

- Bewsher *et al.* (2010) used fits to star intensities in NOMAD to derive large-scale flat-field corrections for the HI-1 cameras. These were derived as look-up tables of correction factors for each image bin, rather than as a parameterized relationship. A correction to the photometric conversion factors allowing for the variation in solid angle per pixel across the FOV, taking into account the AZP projection, was also derived.

- Tappin, Eyles & Davies (2015) used fits to stars in the "Yale bright star catalogue" (Hoffleit & Warren, 1995) to derive an updated large-scale flat-field correction for the HI-2 cameras using the 5-parameter correction defined in Section A.3.2.3.

  The deviations of the fits to the AZP projection obtained from measured positions of stars in the HI-2 cameras were also examined. It was shown that there are systematic effects but the deviations are ≤ 1 image bin within the optimized circular field-of-view (*i.e.* out to bin radius 512, or approximately 35 degrees), with deviations up to ~ 4 bins in the corners of the image.

- Tappin (2017) presented the deviations of the fits to the AZP projection obtained from measured positions of stars for the HI-1 cameras. The fit is excellent with typical deviations << 1 image bin across the entire FOV (including corners).

A.3.3.2 Validation

The calibrations and corrections described in this section have been derived from detailed analysis of pre-launch and in-orbit data from the HI instruments. They have been validated by comparing stellar positions in the corrected images with their known position in astrometric catalogues.

A.3.4 References

Bewsher, D., Brown, D.S., Eyles, C.J., Kellet, B.J., White, G.J., Swinyard, B.: 2010, Determination of the photometric calibration and large-scale flatfield of the STEREO Heliospheric Imagers: I. HI-1, *Solar Phys.* **264**, 433-460.

Brown, D.S., Bewsher, D., Eyles, C.J., 2009, Calibrating the pointing and optical parameters of the STEREO Heliospheric Iagers, *Solar Phys*. **254**, 185-225.

Calabretta, M.R., Greisen, E.W., 2002, Representations of celestial coordinates in FITS, *Astron. Astrophys*., **395**, 1077-1122.

Eyles, C.J., Harrison, R.A., Davis, C.J., Waltham, N.R., Shaughnessy, B.M., Mapson-Menard, H.C.A., Bewsher, D., Crothers, S.R., Davies, J.A., Simnett, G.M., Howard, R.A., Moses, J.D., Newmark, J.S., Socker, D.G., Halain, J.-P., Defise, J.-M., Mazy, E., Rochus, P.: 2009, The Heliospheric Imagers onboard the STEREO mission, *Solar Phys*. **254**, 387-445.

Halain, J.-P., 2012, *PhD Thesis*, Section 4.3, Université de Liége, Belgium.

Hoffleit, D., Warren, W.H. Jr., 1995, VizieR Online Data Catalog: Bright Star Catalogue, 5th Revised Ed. (Hoffleit+, 1991), *VizieR Online Data Catalog* 5050.

Tappin, S. J., Eyles, C. J., Davies, J. A., 2015, Determination of the photometric calibration and large-scale flatfield of the STEREO Heliospheric Imagers: II. HI-2, *Solar Phys*, **290**, 2143-2170.

Tappin, S.J., 2017, Considerations for the use of STEREO-HI data for astronomical studies, *Astron. J.* **153**, 4, 164.

Zacharias, N., Monet, D.G., Levine, S.E., Urban, S.E., Gaume, R., Wycoff, G.L., 2004, The Naval Observatory merged astrometric dataset (NOMAD), *Bulletin Amer. Astron. Soc.* **36**, 1418.

A.4 Background determination

A.4.1 Overview

In common with all solar coronagraphs, there is a real challenge in determining the background that needs to be subtracted in order to extract the solar wind signal, including that of CMEs, from other sources. An additional issue with HI is the relatively low image cadence, required to mitigate the reduced Thomson scattered signal far from the Sun. After some experimentation, a robust statistical solution was found, based on the mean of the running lower quartile of the Level 1 data, to determine the stable background (F-corona and stray light). This background is calculated on an image bin by image bin basis (with a correction for pointing offsets – see below). To satisfy competing scientific requirements, we produce 1-day and 11-day backgrounds for HI-1 to either remove or retain longer-lived solar wind structures (such as the streamer belt), respectively. For HI-2, a 1-day background creates artefacts around stellar sources since the stars do not move far enough through the field of view and so a 3-day background is generated instead. Figure 3 shows the Level 1 signal along the horizontal center of a sample HI-1 image (black line), and the corresponding signal with a 1-day running background removed (Level 2; red line).

In producing the data stack for the background calculation, a number of operational filters are applied:

- Images with more than 15 missing telemetry blocks are rejected – these adversely affect the shutterless correction, resulting in an apparent brightening in the rest of the column.
- Images where the pointing calibration is poor or failed are rejected.
- Images where the spacecraft is rolled from the nominal pointing are rejected.
- Images where the number of summed frames is outside the limits 20-40 for HI-1 and 80-110 for HI-2 are rejected.

- Columns where probable saturation has occurred are masked as are the adjacent columns due to potential issues with bleeding in the readout register (see Section 2.1.2).

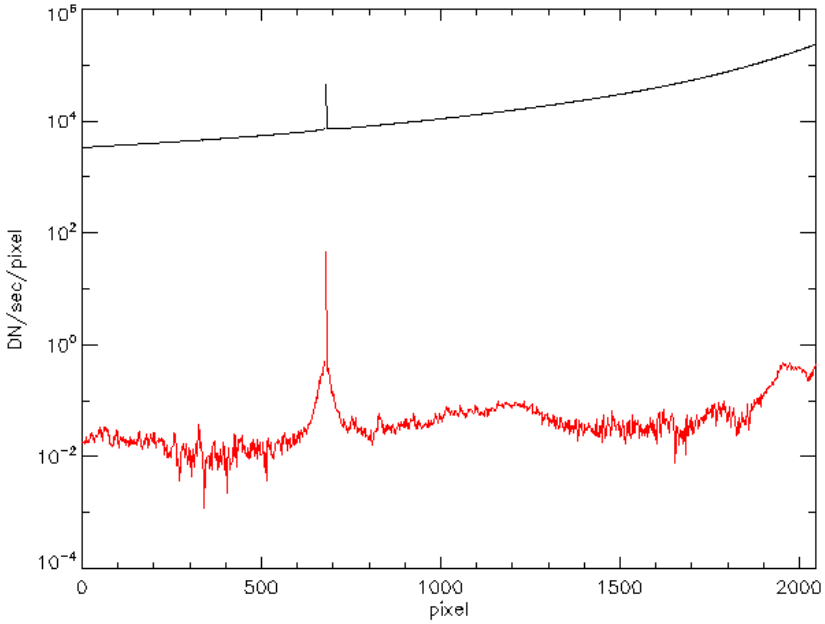

Figure 3. Level 1 signal (black) and Level 2 signal (red) along the horizontal center of the HI-1A field of view.

A similar plot for HI-2 is shown in Figure 4. The dip on the left hand side is a result of the inclusion of the so-called Earth occulter as the instrument design (see Eyles et al., 2009).

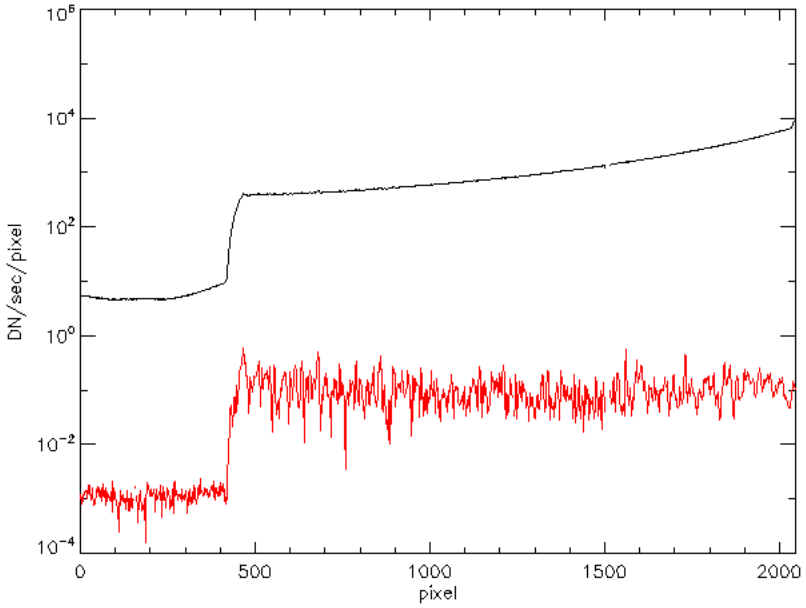

Figure 4. Similar to Figure 3, for HI-2.

There is an additional issue with HI-1B in that occasionally the camera pointing becomes temporarily slightly unstable at a level that can cause movement of the image of a few bins (Tappin, 2017). To mitigate this effect, we check if the movement between the alignment of images in the stack used to generate the background is different by more than 1 bin to that expected. If that is the case, the stack is interpolated using the fitted pointing data to bring the data back to the expected pointing. For HI-2B, it is more challenging to get the pointing data to the required accuracy though in general it seems to be less of an issue in that data.

A.4.1.1 Heritage

The lower quartile subtraction method owes much to the work of Andrew Buffington, developed for the SMEI instrument (see Jackson et al., 2004), who recommended it as a statistically robust technique.

A.4.1.2 Product Description

The different kinds of background-subtracted data (Level 2 data) produced from HI data:

1 Day – HI-1 only, file names end '_br01'

3 Day – HI-2 only, files names end '_br03'

11 Day – both cameras, files names end '_br11'

Data is also provided in different units. Thus the options for the *last portion* of the Level 2 filenames can be given as:

_2<x>h<1|2><a|b>_br<nn>

Where x can be:

4 – data is still in units of DNS

b – data is in units of MSB

t – data is in S10 units.

The term nn is '01', '03' or '11' and the vertical line (|) indicates 'or'.

For example, the file ending would be:

'_24h1a_br01' for HI-1A data in units of DNS with a 1-day background subtracted

'_2bh2a_br11' for HI-2A data in units of MSB with an 11-day background subtracted

'_2th2b_br01' for HI-2B data in S10 units with a 3-day background subtracted

'_2bh1b_br11' for HI-1B data in units of MSB with an 11-day background subtracted

Figure 5 shows a sample HI-1A image without and with background subtraction. Note that, as well as the aforementioned processing to Level 2, SwRI has their own L2 processing pipeline (DeForest, Howard and Tappin, 2011).

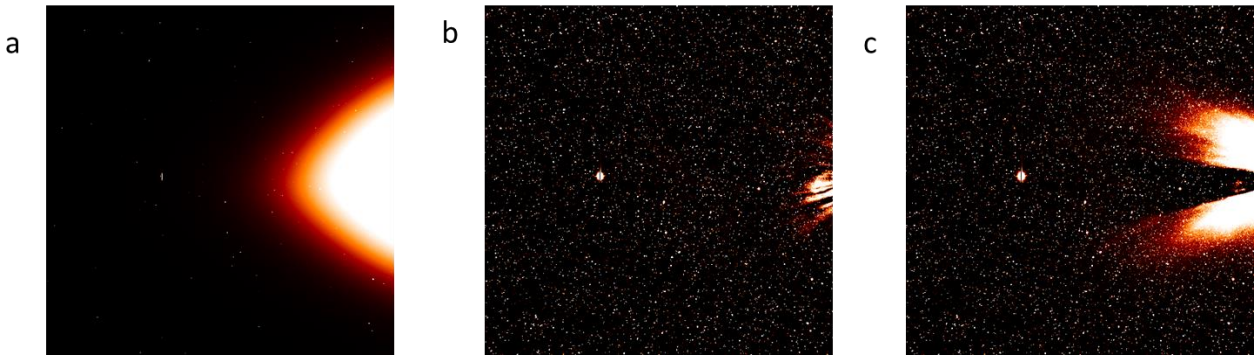

Figure 5. Images before and after background subtraction. a) Level 1 data (scaled 5 orders of magnitude greater than subsequent panels) (b) Level 2 data with 1-day background subtracted (c) Level 2 data with 11-day background subtracted.

A.4.2 Error Analysis and Corrections

Movies are produced routinely for the images and can be a useful way of detecting issues in the raw data. In particular with HI-1B images, it is sometimes necessary to filter images where the pointing has changed mid exposure.

A.4.3 Calibration and Validation

A.4.3.1 Calibration

Background-subtracted HI-1 images have been compared with the data obtained from the COR2 coronagraphs.

A.4.3.2 Validation

By aligning images using the pointing calibration, it is possible to significantly reduce the moving stellar sources in the field of view making the detection of transient sources easier.

A.4.4 References

DeForest, C.E., Howard, T.A., Tappin, S.J, 2011, Observations of detailed structure in the solar wind at 1 AU with STEREO/HI-2, *Astrophys. J*, **738**, 103.

Jackson, B.V., Buffington, A., Hick, P.P., Altrock, R.C., Figueroa, S., Holladay, P.E., Johnston, J.C., Kahler, S.W., Mozer, J.B., Price, S., Radick, R.R., Sagalyn, R., Sinclair, D., SImnett, G.M., Eyles, C.J., Cooke, M.P., Tappin, S.J., Kuchar, T., Mizuno, D., Webb, D.F., Anderson, P.A., Keil, S.L., Gold, R.E., Waltham, N.R.: 2004, The Solar Mass Ejection Imager (SMEI) mission, Solar Phys. **225**, 177-207.

Tappin, S.J., 2017, Considerations for the use of STEREO-HI data for astronomical studies, *Astron. J.* **153**, 4, 164.